

Article

Resource Recycling Utilization of Distillers Grains for Preparing Cationic Quaternary Ammonium—Ammonium Material and Adsorption of Acid Yellow 11

Chengtao Li ^{1,*}, Deyi Kong ¹, Xiaolong Yao ², Xiaotao Ma ¹, Chunhui Wei ³ and Hong Wang ⁴

¹ College of Environmental Science and Engineering, Shaanxi University of Science & Technology, Xi'an 710021, China; kdy2929491809@163.com (D.K.); hanjhjh@163.com (X.M.)

² Key Laboratory of Cleaner Production and Integrated Resource Utilization of China National Light Industry, Beijing Technology and Business University, Beijing 100048, China; yaoxiaolong@btbu.edu.cn

³ Liquor Making Biological Technology and Application of Key Laboratory of Sichuan Province, Sichuan University of Science & Engineering, Zigong 643000, China; wei_chunhui@suse.edu.cn

⁴ Key Laboratory of Wuliangye-Flavor Liquor Solid-State Fermentation, China National Light Industry, Yibin 644000, China; wanghong@wuliangye.com.cn

* Correspondence: lichengtao@sust.edu.cn

Abstract: Using distillers grains (DG) as raw material after pre-treatment with sodium hydroxide (NaOH) and modified with cationic etherification agent 3-chloro-2-hydroxypropyltrimethylammonium chloride (CHPTAC), cationic quaternary ammonium distillers grains adsorption material (CDG) was successfully prepared. The optimal adsorption conditions were an adsorption temperature of 25 °C, adsorption time of 180 min, amount of adsorbent at 8.5 g/L, initial dye concentration of 100 mg/L, and pH of dye solution 7.0. The structure of CDG was characterized by FTIR, EDS, SEM, BET, ultraviolet spectrum analysis, and analysis of the zeta potential, while the adsorption mechanism was studied by adsorption kinetics, isotherms, and thermodynamics. The results showed that CHPTAC modified the distillers grains successfully and induced the formation of CDG with a large number of pore structures and good adsorption effect. The highest adsorption yield was above 98%, while after eight rounds of adsorption–desorption experiments, the adsorption rate was 81.80%. The adsorption mechanism showed that the adsorption process of acid yellow 11 (AY11) by CDG conforms to the pseudo-second-order kinetic model, mainly with chemical and physical adsorption such as pore adsorption and electrostatic adsorption. Thermodynamics conforms to the Freundlich isothermal model, and the adsorption process is a spontaneous, endothermic and entropy-increasing process.

Keywords: distillers grains; acid dyes; adsorption mechanism; solid waste recycling utilization



Citation: Li, C.; Kong, D.; Yao, X.; Ma, X.; Wei, C.; Wang, H. Resource Recycling Utilization of Distillers Grains for Preparing Cationic Quaternary Ammonium—Ammonium Material and Adsorption of Acid Yellow 11. *Sustainability* **2022**, *14*, 2469. <https://doi.org/10.3390/su14042469>

Academic Editors: Rajesh Kumar Jyothi and Antonio Caggiano

Received: 19 December 2021

Accepted: 14 February 2022

Published: 21 February 2022

Publisher's Note: MDPI stays neutral with regard to jurisdictional claims in published maps and institutional affiliations.



Copyright: © 2022 by the authors. Licensee MDPI, Basel, Switzerland. This article is an open access article distributed under the terms and conditions of the Creative Commons Attribution (CC BY) license (<https://creativecommons.org/licenses/by/4.0/>).

1. Introduction

At present, the excessive use of dyes and large amounts of emissions are not only causing water pollution but also could threaten human health, therefore the subject has attracted increased attention from scholars. Data show that more than 700,000 tons of organic dyes are produced every year [1], of which about 35,000 to 70,000 tons of organic dyes are released in wastewater without any treatment [2]. Azo dyes are the most important class of synthetic dyes and pigments, accounting for 60–80% of all organic colorants. They are widely used on substrates such as textile fibers, leather, plastics, paper, hair, mineral oil, wax, food, and cosmetics [3–6]. When wastewater with the azo dye enters a body of water, it could hinder the penetration of light and seriously affect aquatic organisms [7]. At the same time, dyes can contaminate groundwater and eventually enter into the human body, causing health problems, as most azo dyes are toxic and/or carcinogenic [8]. Therefore, looking for a cost-efficient method for azo dye wastewater treatment has become a demand of today's society and industry.

In the dye industry, several wastewater treatment methods have been applied in order to remove azo dyes, based on electrochemical treatment [9], flocculation [10], chemical oxidation [11], liquid–liquid extraction [12], biological oxidation [13], ion exchange [14], photocatalytic degradation [15], precipitation [16], adsorption [17] and membrane separation [18]. The adsorption method [19] is widely used to remove organic dyes from wastewater due to its fast decolorization and simple operation. In addition, more and more materials are used as adsorbents, such as silica-based materials [20], metal oxides [21], activated carbon [22], zeolite [23], alumina [24], silica [25], biomaterials [26], and polymers [27]. However, the adsorbents mentioned above still have the disadvantages of poor selectivity, inconvenient separation, difficult recovery, and high cost. Therefore, searching for new adsorbents with high adsorption capacity, high stability, low cost, and recyclability has become a current hotspot of investigations.

Acid yellow 11 (AY11) is an azo dye in acid dyes [28–30], yellow powder, and its structural formula is shown in Figure 1. Its molecular structure contains an azo group (-N=N-), being easily soluble in water as an anionic dye. The AY11 dye contamination of wastewaters has the characteristics of high chroma, high chemical stability, and high resistance toward biodegradation, being harmful to the environment and human health.

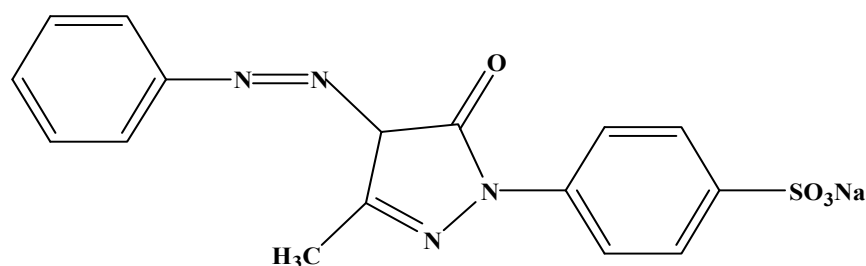


Figure 1. Structural formula of AY11.

Cellulose is one of the most widespread biological macromolecules in nature [31]. Therefore, it can be considered as an inexpensive, biodegradable, and renewable biopolymer, which has received extensive attention due to its unique physical and chemical properties [32]. Despite various advantages, natural cellulose itself does not have a high adsorption capacity if it is directly used as an adsorbent without modification. In these cases, the adsorption capacity may be low and the selectivity is poor [33]. Therefore, in order to improve its adsorption capacity, many investigations have concentrated on the modification of cellulose through esterification, etherification, or graft copolymerization in order to improve the adsorption capacity and the renewable ability of cellulose.

Distillers grains (DG) are the main by-product in the production process of liquor, which contains cellulose as its main component [34]. At present, DG are mainly used directly as feed in livestock farming, but the rate of usage is low, resulting in a large amount of DG accumulation. At the same time, fresh DG have high water content, are perishable and deteriorate, and long-term accumulation will cause not only a severe waste of resources but also environmental pollution. The use of waste distillers grains to prepare adsorbent materials could not only solve the problem of resource optimization and utilization of DG, but also could use waste distillers grains as raw materials for adsorbents.

Quaternary ammonium salt is a relatively common cationic compound that can interact with negatively charged substances on the surface. At present, trimethylamine [35], 3-chloro-2-hydroxypropyl trimethylammonium chloride [36], and tetraacetylenediamines [37] were used to prepare quaternized cationized cellulose, used as an adsorbent to treat anionic dye wastewater [38].

Therefore, in this study, the cationic etherification agent 3-chloro-2-hydroxypropyltrimethylammonium chloride (CHPTAC) was used to modify the alkalinized distillers grains to obtain a cationic distillers grain adsorbent (CDG). The applied etherification process could introduce a quaternary ammonium cationic group (-N(CH₃)₃) on the long cellulose chain, which

strengthens the electrostatic interaction between the anionic group in CDG ($-\text{SO}_3^-$) and the AY11 molecule. At the same time, the introduction of new groups may expand the molecular structure and increase its contact site and area with the AY11 molecule, thereby improving the adsorption rate of CDG to AY11 component of the wastewater. This study could also provide a theoretical basis for the recycling of biological waste and the application of waste DG as an adsorbent in the removal of azo dye wastewater, realizing the environmental protection concept of “treatment of waste by waste”.

2. Materials and Methods

2.1. Materials and Chemicals

In the present investigation, the used DG were obtained from a winery in Xi’an, Shaanxi (China). Chemical reagents included analytically pure sodium hydroxide (NaOH), hydrochloric acid (HCl), 3-chloro-2-hydroxypropyl trimethylammonium chloride (CHPTAC), acid yellow 11 (AY11) and absolute ethanol ($\text{CH}_3\text{CH}_2\text{OH}$). The water used was distilled water.

2.2. Pre-treatment of DG and Preparation of CDG

To begin, 15 g of 120 mesh of DG powder was introduced into a 250 mL three-necked flask with 200 mL, 10% NaOH solution. In the next step, the reaction mixture was placed on a water bath at 30 °C, 110 RPM for 180 min. When the reaction was completed, the as-obtained mixture was filtered with distilled water and 95% ethanol solution, washed until reaching neutrality, and dried completely in an oven at 60 °C to obtain the alkalized DG. Then, the alkalized DG were introduced in a 250 mL three-necked flask, adding 200 mL of NaOH solution with a mass fraction of 20%, and reacting at 30 °C, 110 RPM on a water bath for 120 min, and CTA was added to continue the reaction. After the reaction was completed, it was filtered and washed with 95% ethanol and distilled water again, until reaching the neutral pH, and dried in an oven at 60 °C to obtain CDG. The schematic diagram of the reactions [29] are shown in Figure 2.

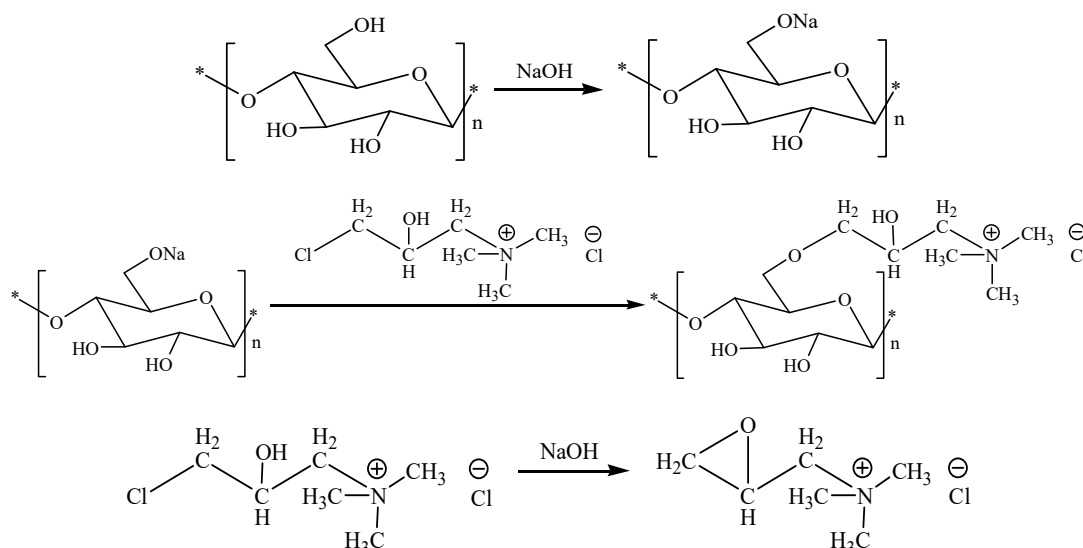


Figure 2. Schematic diagram of CDG synthesis (* the terminal group).

2.3. Characterization of CDG

The Vector-22 Fourier Transform Infrared Spectrometer (FTIR) (Vector-22, Bruker, Karlsruhe, Germany) was used to analyze the functional groups of CDG. The scanning range was set $4000\text{--}500\text{ cm}^{-1}$, and the number of scans was 32. The energy dispersive spectrometer (EDS) (EDAX Octane Prime, EDAX, Mahwah, NJ, USA) was used to analyze the type and content of the component elements in the material micro area. The surface

morphology of CDG was observed by FEI Q45 scanning electron microscope (SEM) (FEI-Q45, FEI, Hillsboro, OR, USA).

The Brunauer–Emmett–Teller (BET) (ASAP2460, Mike Corporation, Norcross, GA, USA) was used to study the surface area and the porosity of DG and CDG; this analysis was carried out by N2 adsorption–desorption isotherm and the surface area was calculated by BET plot. UV-2006A ultraviolet-visible spectrophotometer (UV-2006A, Brucher, German) measured the absorbance of the solution after adsorption; the surface charge of CDG was analyzed using a zeta potentiometer (zeta potential) (JS94HM, ZKT, Shanghai, China). The conditions of the zeta potential determined CDG were concentration 40 % *w/v*, temperature 25 °C, the average size of the dispersed particles was 80–160 μm, the sample surfaces were probed with either aqueous 1 mM KCl solution, 0.05 M KOH solution to raise the pH, or 0.05 M HCl to decrease the pH to 4. The zeta potential was determined by the Helmholtz–Smoluchowski Equation (1) [39]:

$$\zeta = \frac{dI}{dP} \frac{\eta}{\zeta_r \zeta_0} \frac{L}{A} \tag{1}$$

where *dI* is the differential streaming current, *dP* is the differential pressure drop, *η* is the solution viscosity, *ζ_r* is the solution relative permittivity, *ζ₀* is the vacuum permittivity, *L* is the length of the streaming channel, *A* and is the cross-section of the streaming channel.

2.4. Batch Adsorption Experiment

The adsorption performance of CDG toward AY11 dye was investigated by the addition of 0.13 g of CDG to 20 mL of AY11 dye solution, containing 200 mg of coloring agent per 1000 mL aqueous solution, and by changing the adsorption temperature (25–45 °C), adsorption time (40–290 min), the amount of adsorbent (1.5–10.5 g /L), the initial concentration of AY11 (50–400 mg/L), and the pH of adsorption (1.0–9.0, adjusted by adding 1 M NaOH or 1 M HCl). The adsorbent was dispersed entirely into the solution at a constant temperature and with a specific adsorption time, the condition was showed as Table 1. After the adsorption process, the CDG was centrifuged and separated from the supernatant, and distilled water was used as a control. The absorbance was measured at 417 nm with an ultraviolet spectrophotometer, and the residual concentration/absorption rate of the dye was calculated using the following equations:

$$q_e = \frac{(C_0 - C_e) \times V}{m} \tag{2}$$

$$\eta = \frac{C_0 - C_e}{C_0} \times 100\% \tag{3}$$

where *C₀* and *C_e* were the initial concentration of AY11 and the concentration after the adsorption process (mg/L), *V* was the initial volume of the dye (mL), *m* was the amount of adsorbent (g), *q_e* was the adsorption capacity (mg/g), and *η* was the efficiency of removal.

Table 1. The effect of factors on the adsorption effect of AY11 on CDG.

	The Effect of Temperature	The Effect of Time	The Effect of Mass of CDG	The Effect of Initial Concentration of AY11	The Effect of pH
temperature/°C	25, 30, 35, 40, 45	25	25	25	25
time/min	180	30, 60, 90, 120, 180, 240, 300	180	180	180
the mass of CDG/ g/L	6.5	6.5	1.5, 2.5, 3.5, 4.5, 5.5, 6.5, 7.5, 8.5, 9.5, 10.5	6.5	6.5
the initial concentration of AY11/mg/L	200	200	200	50, 100, 150, 200, 250, 300, 350, 400	200
pH	7	7	7	7	1, 2, 3, 4, 5, 6, 7, 8, 9

2.5. Regeneration Performance

The CDG after adsorption was soaked in 0.1 mol/L NaOH solution and shaken at 180 RPM for 10 min. Afterward, it was washed five times with deionized water and dried in a vacuum oven at 60 °C to obtain the regenerated CDG. In the last step, adsorption experiments were conducted to analyze the ability of the regenerated CDG to adsorb AY11. In order to investigate the reusability of CDG, the adsorption–desorption cycle was repeated eight times.

2.6. Adsorption Mechanism

2.6.1. Adsorption Kinetic Model

The kinetic model in the adsorption process mainly investigates the change in the adsorption amount with time and obtains the relationship between the adsorption amount and time, using a kinetic model to fit [40]. Pseudo-first-order kinetic models and pseudo-second-order kinetic models are commonly used as solid–liquid adsorption kinetic models [41].

Pseudo-first-order kinetics [42] were first used to study the variation of the adsorption amount with the adsorption time, using the following Equation (4):

$$q_t = q_e(1 - e^{-k_1 t}) \quad (4)$$

The pseudo-second-order kinetic model was used to describe the adsorption capacity of the adsorbent [43], using the following Equation (5):

$$q_t = \frac{k_2 q_e^2 t}{1 + k_2 q_e t} \quad (5)$$

where q_e and q_t were the adsorption capacities at adsorption equilibrium (mg/g); k_1 was the pseudo-first-order adsorption rate constant (min^{-1}), and k_2 was the pseudo-second-order adsorption rate constant, ($\text{g/mg} \cdot \text{min}^{-1}$).

2.6.2. Adsorption Isotherm Model

The adsorption isotherm model was used to describe the relationship between the adsorption amount and the equilibrium concentration of the solution when the adsorption reached the equilibrium at a specific temperature, from which the interaction mechanism between the adsorbent and the adsorbate can be inferred, and it could also be used to select the optimal adsorption agent [44].

The adsorption isotherm represents the distribution of adsorbed molecules between the liquid and solid phase when the adsorption reaches its equilibrium [45]. The establishment of a more suitable balance curve could optimize the adsorption system [45].

The Langmuir adsorption isotherm model assumes that molecular adsorption is a process of monomolecular surface adsorption; the surface of the adsorbent is uniform and has some of the same adsorption sites. When the kinetics reach equilibrium, no further adsorption occurs and the adsorbed particles are completely independent from other adsorption particles, as there is no interaction between them [46,47], as described by Equation (6):

$$q_e = \frac{abC_e}{1 + aC_e} \quad (6)$$

where C_e (mg/L) was the concentration of the equilibrium, q_e (mg/g) was the equilibrium adsorption capacity at this concentration.

The Freundlich adsorption isotherm is an empirical equation which could be used to predict whether or not the adsorbent surface is uniform; if it is not, the adsorption amount increases with the increase in solution concentration, and there is an interaction force between the adsorbed molecules [48,49], as described in Equation (7):

$$q_e = K_F C_e^{\frac{1}{n}} \quad (7)$$

where C_e (mg/L) is the equilibrium concentration, and q_e (mg/g) is the equilibrium adsorption capacity at the concentration. K_F (L/mg) is the Freundlich adsorption constant related to the adsorption capacity, which characterizes the strength of the interaction between the adsorbent and the dye (the higher the K_F means higher adsorption capacity of the adsorbent). $1/n$ is the non-uniformity factor of the Freundlich model and represents the adsorption strength. When $0 < 1/n < 1$, it indicates that the adsorption process was favorable and easy to proceed; if $1/n = 1$, the adsorption reaction was linear and there was no interaction between the adsorbates; when $1/n > 1$, adsorption, the process is negative, and the adsorption reaction is more difficult.

2.6.3. Adsorption Thermodynamic Model

The adsorption thermodynamic model investigates the effect of the temperature of the solution, which is adsorbed at different solution concentrations. The related thermodynamic parameters [50] (ΔG_0 , ΔS_0 , ΔH_0) are described in Equations (8) and (9):

$$\Delta G_0 = -RT \ln K \quad (8)$$

$$\ln K = \frac{\Delta S_0}{R} - \frac{\Delta H_0}{RT} \quad (9)$$

$$K = \frac{q_e}{C_e} \quad (10)$$

where T is the temperature (K); R is gas constant, and K is the adsorption equilibrium constant, C_e (mg/L) is the concentrations of adsorption equilibrium, and q_e (mg/g) is the adsorption capacity of adsorption equilibrium.

3. Results and Discussion

3.1. FTIR Analysis of DG and CDG

The FTIR spectra of DG and CDG are shown in Figure 3. It can be seen that the spectra of CDG and DG are basically similar; the small differences are as follows:

For CDG, the peaks appearing at 3550 cm^{-1} and 3650 cm^{-1} could be attributed to the O-H stretching vibration of the hydroxyl group [51], as the hydrogen bond was destroyed during the modification process, the internal structure of the DG was opened, and the hydroxyl groups in the DG were exposed.

The absorption peak at 1060 cm^{-1} was enhanced due to the change in absorption peak of the C-O-C bond on the molecular chain of the quaternized product [52].

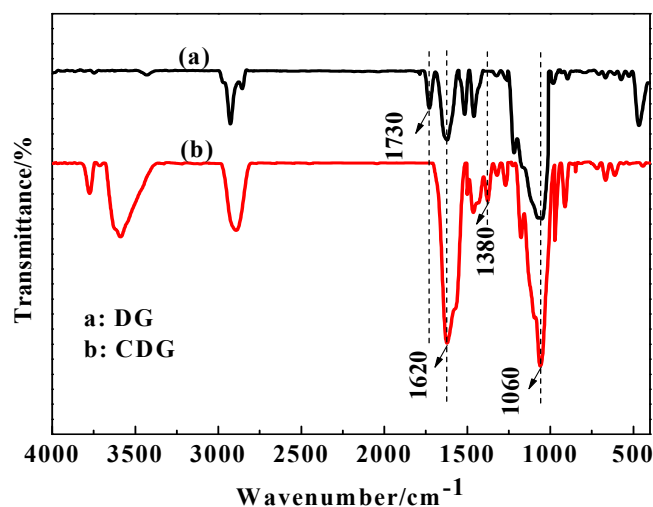


Figure 3. FTIR spectra of (a) DG and (b) CDG.

The characteristic absorption peak of C-N at 1380 cm^{-1} for CDG indicates that the C-N functional group was successfully introduced into the DG, while the absorption peak of CDG at 1620 cm^{-1} was also significantly enhanced, which could be attributed to the presence of -CH₃ in the quaternary ammonium salt, which undergoes bending oscillation. The absorption peak at 1730 cm^{-1} disappeared, which could have been caused by the bending vibration of the alcoholic hydroxyl group. These results indicate that the CHPTAC successfully modified the DG, and CDG was successfully obtained.

3.2. EDS Structure Characterization of DG and CDG

The EDS images of DG and CDG can be observed in Figure 4. We can see that the mass percentage of C element in the CDG increased by 15.15%, O element increased by 19.05%, and N element increased by 3.47%. The main reason is that DG is mainly composed of C, H, and O elements, and -N(CH₃)₃ group is introduced when CTA modifies DG, and NaOH participates in the ring-opening reaction as a catalyst during the modification process. This result shows that CTA modified DG successfully, and further corroborates the characterization results of FTIR.

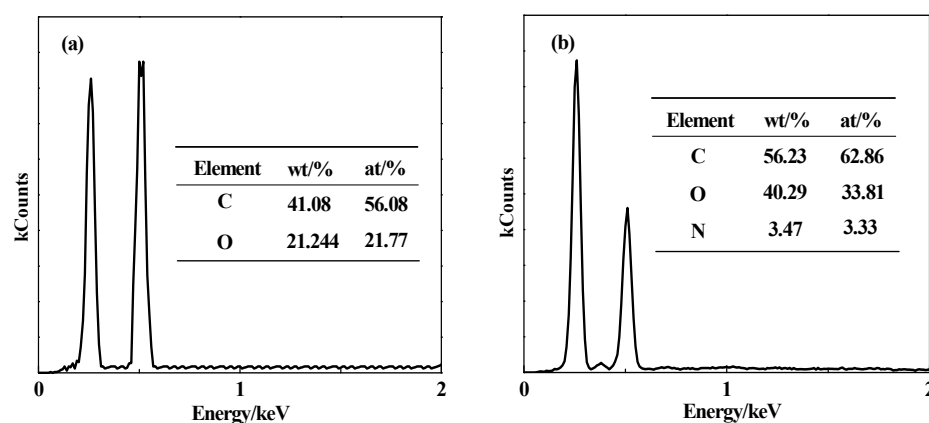


Figure 4. EDS spectra of (a) DG and (b) CDG.

3.3. SEM Analysis of DG and CDG

The SEM images of DG and CDG can be observed in Figure 5. It can be seen that the surface of DG is smooth and has a dense structure of lignocellulose fibers; however, many pore structures appeared on the surface of CDG. This could be attributed to the fact that the cell wall in CDG was modified by alkali treatment and became loose and swollen, increasing the porosity. After modification, the ability of mass transfer of CDG was improved, and more adsorption and binding sites were exposed on the surface, which could be beneficial to the entry of AY11 dye molecules, improving in this way the adsorption performance of CDG.

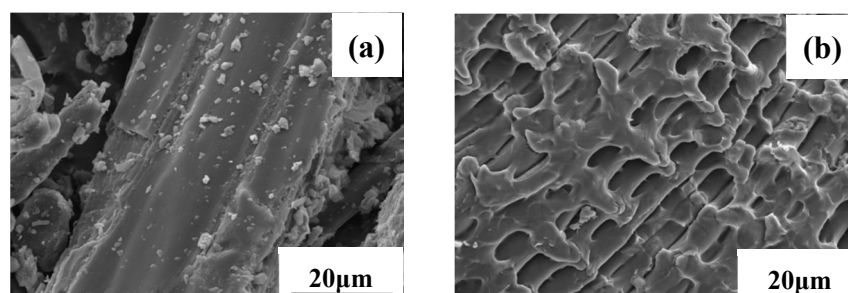


Figure 5. SEM micrographs of (a) DG and (b) CDG.

3.4. The BET Analysis of CDG

Figure 6 shows the N₂ adsorption–desorption curves of DG and CDG (a) and the pore size distribution (b). The N₂ adsorption–desorption curves of DG and CDG are both typical Type IV [53]. As can be seen from Figure 6a, when P/P₀ is less than or equal at 0.4, the adsorption and desorption curves of DG overlap, indicating the presence of microporous and monolayer adsorption. When P/P₀ is greater than 0.4, the adsorption of CDG to N₂ increases rapidly, indicating that the pores in the adsorbent are slit pores [54]. As can be seen from Figure 6b, the pore size distribution of DG is 5–100 nm, while the CDG distribution is 10–40 nm. After modification, the specific surface area and pore volume of DG become larger, which is consistent with the results in Table 2. The specific surface area of CDG is 3.51 m²/g. Compared with DG, the specific surface area is increased by 242%, indicating that the increase in the specific surface area of CDG is beneficial to the adsorption of dyes.

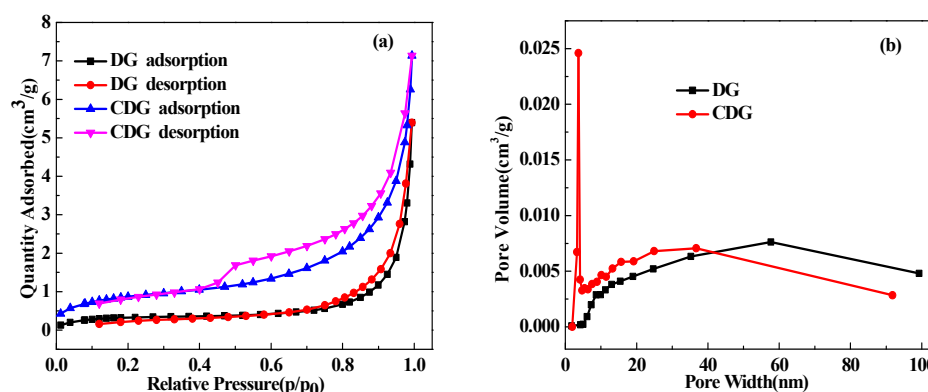


Figure 6. N₂ adsorption–desorption curves of DG and CDG (a) and pore size distribution (b).

Table 2. Specific surface area parameters of DG and CDG.

Sample	BET Surface Area (m ² /g)	Pore Volume (cm ³ /g)	Average Pore Size (nm)
DG	1.09	6.3 × 10 ^{−5}	29.42
CDG	3.51	1.19 × 10 ^{−4}	20.93

3.5. Zeta Potential Analysis of DG and CDG

Figure 7 shows the difference in zeta potential between DG and CDG at different pH values. It can be observed that in the same pH range, the Zeta potential of the CDG was increased. This is because the DG fiber before modification had a large amount of electronegative -OH. The CDG fiber modified by the CTA introduced a large number of positively charged -N(CH₃)₃ groups, which consumed part of -OH on the DG fiber and reduced the total amount of -OH, resulting in electrical transformation, making the Zeta potential of CDG positive [55]. AY11 is an anionic dye with good affinity for cationic substances under the action of electrostatic adsorption. Therefore, CDG could adsorb AY11 by electrostatic force.

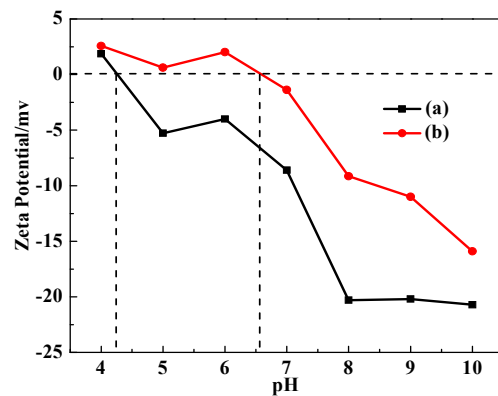


Figure 7. Zeta potential analysis of (a) DG and (b) CDG.

3.6. Adsorption of AY11 on CDG

AY11 was used for adsorption tests at 30 °C. CDG adsorbed 100 mg/L of AY11 solution in 120 min, and the UV–Vis light scanned the solution before and after the adsorption process. The results and the UV–Vis spectrum analysis are shown in Figure 8.

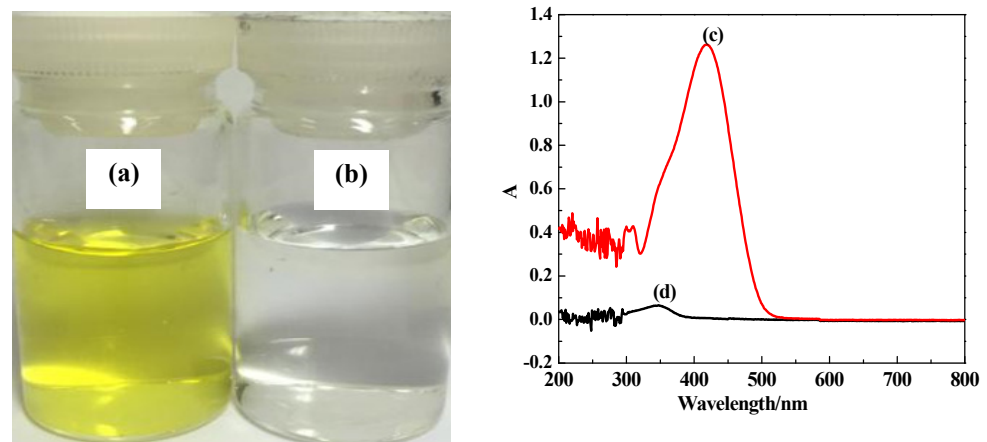


Figure 8. Comparison and UV analysis spectrum of L AY11 solution before and after adsorption by CDG: (a) 100 mg/L AY11 solution, pH = 5.96; (b) 100 mg/L AY11 solution after CDG adsorption, pH = 6.64; (c) UV–Vis spectrum of 100 mg/L AY11 solution; (d) UV–Vis spectrum of 100 mg/L AY11 solution after CDG adsorption.

From Figure 8a,b, it can be found that the solution after adsorption is almost colorless, and the adsorption rate of the dye was 98.76%; as the UV–Vis before adsorption and after adsorption was measured and the absorption peak of the AY11 solution at 417 nm disappeared after adsorption. This result indicates that the AY11 dye in the solution was almost entirely adsorbed, causing the characteristic absorption peak at 417 nm to disappear.

3.7. The Effect of Adsorption Conditions on Adsorption Performance

3.7.1. Adsorption Temperature

When the adsorption temperature was set at 25–45 °C, the adsorption time was 180 min, the mass of CDG was 6.5 g/L, the initial concentration of AY11 was 200 mg/L, and the pH of the solution was 7. The effect of the temperature on the adsorption performance of AY11 could be observed in Figure 9.

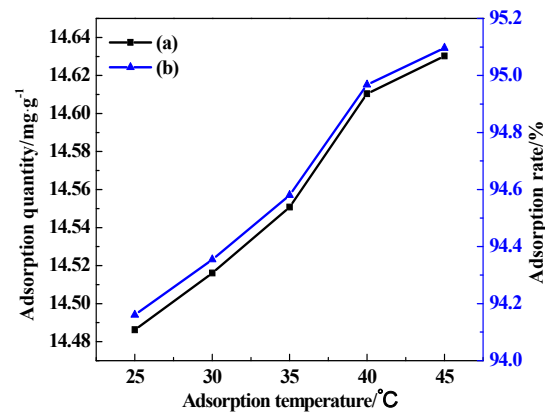


Figure 9. Effect of adsorption temperature on CDG adsorption performance (a) adsorption capacity (b) adsorption removal rate.

It can be seen from Figure 9 that with the increase in temperature, the adsorption removal rate and adsorption amount of AY11 on CDG increased, which proves that the adsorption process could be endothermic, and the increase in temperature is conducive to the adsorption process. However, as the temperature rises, the adsorption removal rate and adsorption amount of AY11 changes only moderately. Therefore, when using CDG to remove the dye from wastewater, the change in temperature of the wastewater will not have a significant effect on the removal rate. According to the actual sewage treatment applications, 25 °C was selected as the optimal adsorption temperature.

3.7.2. Adsorption Time

The effect of adsorption time on the adsorption performance of AY11 (adsorption temperature was set to 25 °C, the mass of CDG was 6.5 g/L, the initial concentration of AY11 was 200 mg/L, and the pH value of the was 7) are shown in Figure 10.

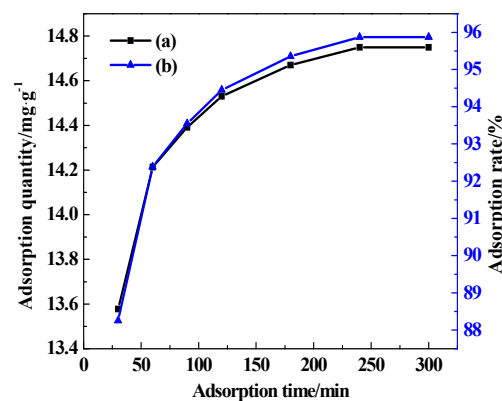


Figure 10. Effect of adsorption time on CDG adsorption AY11 (a) adsorption amount (b) adsorption removal rate.

It can be seen that the removal rate increases rapidly in the initial stage. With the increase in adsorption time, the adsorption of AY11 gradually reached saturation. This is because, at the beginning of adsorption, a large number of free active sites on the surface of the adsorbent are available, but as the adsorption process progresses, the adsorption sites are gradually occupied, and the adsorption rate decreases [56]. On the other hand, as the adsorption time increases, AY11 needs to overcome a higher mass transfer resistance to enter into the interior of the CDG, which leads to a slower absorption rate in the later period. When the amount of adsorbed AY11 and the amount of desorption from the surface of CDG reach a dynamic balance, the adsorption time used in the state is called the equilibrium

time [52]. Equilibrium time is often used to evaluate the affinity of the adsorbent toward the adsorbate.

It can be seen that the adsorption removal rate of AY11 by CDG increased with time, and the adsorption equilibrium was reached at 180 min when the removal rate was 94.44%. According to these results, 180 min was selected as the best adsorption time for further investigations.

3.7.3. Mass of CDG

During the investigations of the mass of CDG (in the range of 1.5 g/L–10.5 g/L), the adsorption temperature was set to 25 °C, the adsorption time was 180 min, the initial concentration of AY11 was 200 mg/L, and the pH of the solution was 7. The effect of the mass of CDG on the adsorption performance of AY11 can be observed in Figure 11.

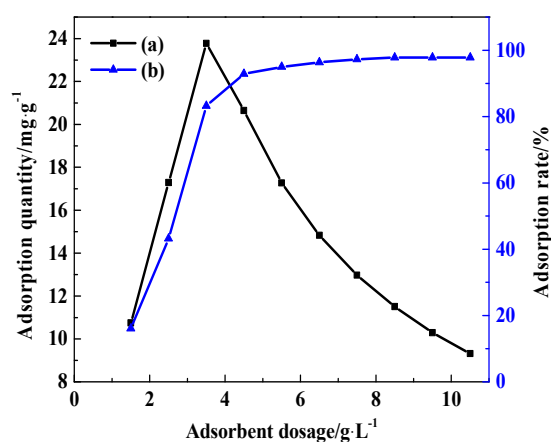


Figure 11. Effect of the mass of CDG on the adsorption of AY11 (a) adsorption amount and (b) adsorption rate.

It can be seen from Figure 11 that with the increase in the mass of CDG, the adsorption rate of AY11 gradually increases. When the mass of CDG was 8.5 g/L, the adsorption reached equilibrium, while the adsorption amount first increased, and then gradually decreased. This could be attributed to the amount of added CDG, where the number of adsorption sites provided to AY11 increases, thereby increasing the adsorption/removal rate of AY11. At the same time, as the amount of added CDG increases, the CDG sheet agglomeration effect increases, the number of active adsorption sites decreases, and the amount of AY11 adsorbed per unit mass of CDG decreases, resulting in a decrease in total adsorption [57]. When the dosage was 8.5 g/L, the adsorption removal rate of AY11 reached 96.66%, but increasing the dosage to 10.5 g/L and the removal rate of AY11 did not change significantly. Therefore, the optimal amount of adsorbent for CDG to adsorb AY11 was found to be at 8.5 g/L.

3.7.4. Initial Concentration of AY11

The effect of the initial concentration of AY11 was investigated in the range of 50–400 mg/L, when the adsorption temperature was set to 25 °C, the adsorption time was 180 min, and the pH of the solution was 7 (Figure 12).

At 298 K, 303 K, and 308 K, the effect of the initial concentration of AY11 on (Figure 13a) adsorption amount and (Figure 13b) adsorption removal rate is shown in Figure 14. As the concentration of the AY11 solution increased, the adsorption amount increased first and then tended to be stable, while the adsorption removal rate increased first and then decreased. As the initial concentration of AY11 increased, the mass transfer power between the adsorbent and the adsorbate increased, and the adsorption rate increased as more AY11 molecules occupied the adsorption sites on the surface of CDG. When the amount of adsorbent is fixed, the number of active adsorption sites is also fixed. With the increase

in the initial concentration of the AY11 solution, the adsorption sites gradually reach a saturation level, and the adsorption removal rate gradually decreases.

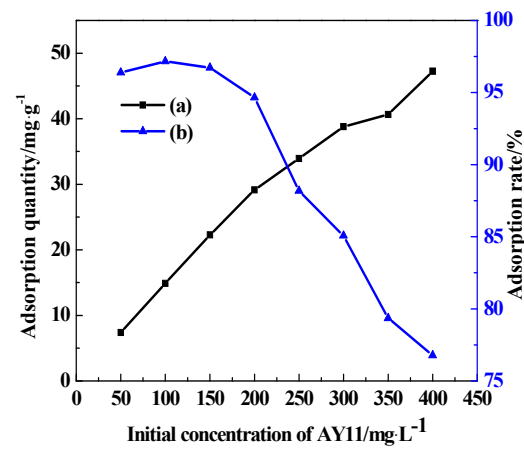


Figure 12. Effect of initial concentration of AY11 on CDG adsorption performance (a) adsorption amount (b) adsorption removal rate.

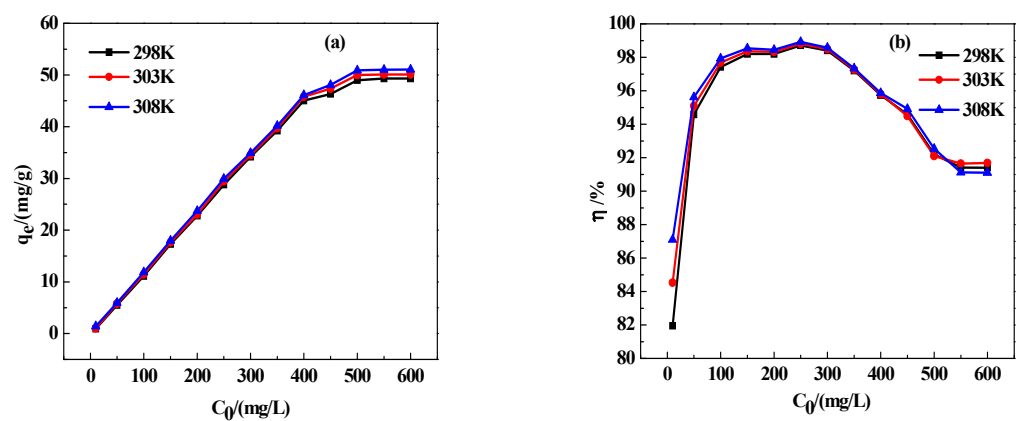


Figure 13. Effect of initial concentration of AY11 on (a) adsorption amount and (b) adsorption removal rate.

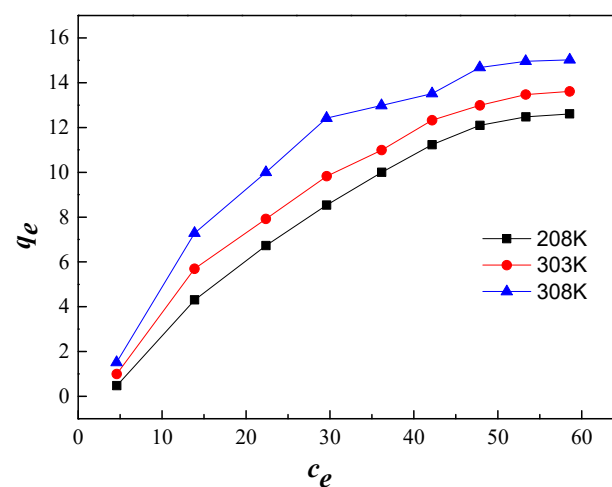


Figure 14. Adsorption isotherms of AY11 onto CDG.

As can be seen from Figure 12, with the increase in the initial concentration of AY11, the adsorption amount of CDG gradually increases, but the adsorption removal rate of AY11

gradually decreases. This could be attributed to the fact that when the initial concentration of AY11 is high, the concentration gradient ($\Delta C = C_0 - C_e$) increases [58], promoting the diffusion of AY11 to the surface and inside of CDG. This increases the probability of AY11 to bind to an adsorption site of CDG, leading to increasing adsorption capacity and resulting in limited adsorption sites in CDG. When the adsorption reaches its saturation, the excess AY11 restricts the spontaneous progress of the adsorption process [59], resulting in a decrease in adsorption removal rate.

Therefore, when the concentration range of AY11 is 50–100 mg/L, the treatment efficiency is the highest with the best applicability.

3.7.5. The Effect of pH

In order to verify the effect of pH toward the removal rate of AY11, the pH of the solution was varied between 1.0–9.0, with an adsorption temperature set to 25 °C, an adsorption time set to 180 min, and an initial concentration of AY11 being 200 mg/L. The effect of pH of AY11 solution on the adsorption performance of AY11 are shown in Figure 15.

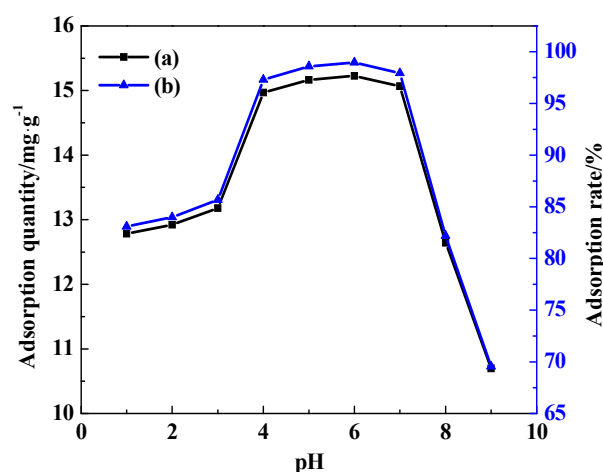


Figure 15. Effect of pH on CDG adsorption performance (a) adsorption capacity and (b) removal rate.

As can be seen from Figure 15, when the pH of the AY11 solution is between 4.0 and 7.0, the adsorption removal rate of AY11 is basically above 95%, indicating that the adsorbent has a wide applicability range for the pH of the dye wastewater. When the initial pH of the solution decreased from 4.0 to 3.0, or increased from 7.0 to 9.0, the removal rate and adsorption amount both decreased rapidly. This is because under strong acid conditions, the higher the H⁺ concentration, the higher the corresponding concentration of Cl⁻, and a large amount of Cl⁻ adheres to the surface of CDG to make it negatively charged, increasing the electrostatic repulsion between the adsorbent and the anionic dye AY11 [60], which prevents AY11 from being adsorbed. Similarly, at higher pH, due to the existence of OH⁻ and the anionic dye, AY11 form a competitive relationship (the presence of OH⁻ and anionic dye AY11 competing for the adsorption sites on CDG) [61], resulting in a rapid reduction in AY11. Therefore, considering the actual pH of the real wastewaters, the optimal initial pH for CDG adsorption of AY11 under these experimental conditions was set to 7.

3.8. Regeneration Performance

In the applicability of wastewater treatment, the low-cost, excellent adsorption efficiency, and renewable adsorbent materials could have significant advantages. Therefore, conducting regeneration experiments is of great significance. Treatment with NaOH solution could reduce the electrostatic interaction between CDG and the anionic dye and could desorb the dye.

The adsorption–desorption cycle of CDG with AY11 was repeated eight times (Figure 16). The adsorption and removal rate of AY11 dye decreased with the increase in cycle time. However, after the 8th adsorption–desorption experiment, the adsorption and removal rate of AY11 by the regenerated CDG still reached 81.80% of the initial results. This shows that CDG has a good regeneration ability, which has excellent application prospects in the treatment of actual dye wastewater.

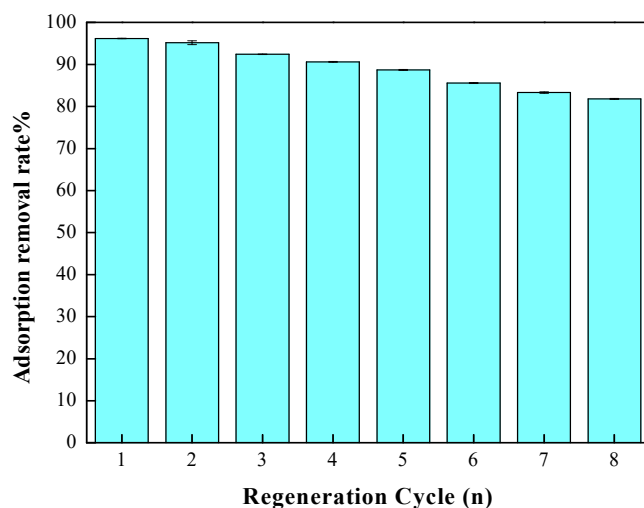


Figure 16. Regeneration performance of CDG.

3.9. Investigations of the Adsorption Mechanisms

The adsorption behavior is usually described by the adsorption model, which has important guiding significance for exploring the interaction mechanisms between the adsorbate and the adsorbent. According to the different ways and forces of interactions between the adsorbent and the adsorbate, the process could be roughly divided into two categories, namely physical adsorption [62] and chemical adsorption [63]. Physical adsorption mainly refers to the van der Waals forces between the adsorbent and the adsorbate, while chemical adsorption mainly plays a role in the chemical bonding force between the adsorbent and the adsorbate. The kinetic model and thermodynamic adsorption model are used to nonlinearly fit the experimental data and analyze the fitting parameters to explore the adsorption mechanism [64].

3.9.1. Adsorption Kinetics

In order to determine the optimal adsorption time, adsorption experiments were carried out at 298, 303 and 308 K, at 10, 30, 60, 90, 120, 180, 240 and 300 min, respectively. The concentration of CDG and AY11 was 8.5 g/L and 100 mg/L, the pH of the AY11 solution was 6.0. The relationship between time and adsorption performance during the adsorption of AY11 on the CDG substrate is shown in Figure 17.

As can be observed, in different adsorption periods, the adsorption amount and adsorption removal rate of AY11 by CDG increased with the increase in adsorption time, and the adsorption amount slowly increased and tended to balance when the adsorption time ≥ 240 min. The adsorption capacity was 38.19 mg/g^{-1} , and the maximum adsorption removal rate was 96.51%. In the initial stage, the concentration gradient of AY11 and the surface of CDG is significant, and there are many adsorption sites on the surface of CDG, and the adsorbate molecules could easily bind with the adsorbent. With the increase in adsorption time, AY11 needs to overcome the mass transfer resistance to enter into the interior of CDG, which reduces the removal rate. With the increase in adsorption time, the adsorption of AY11 gradually reaches its saturation.

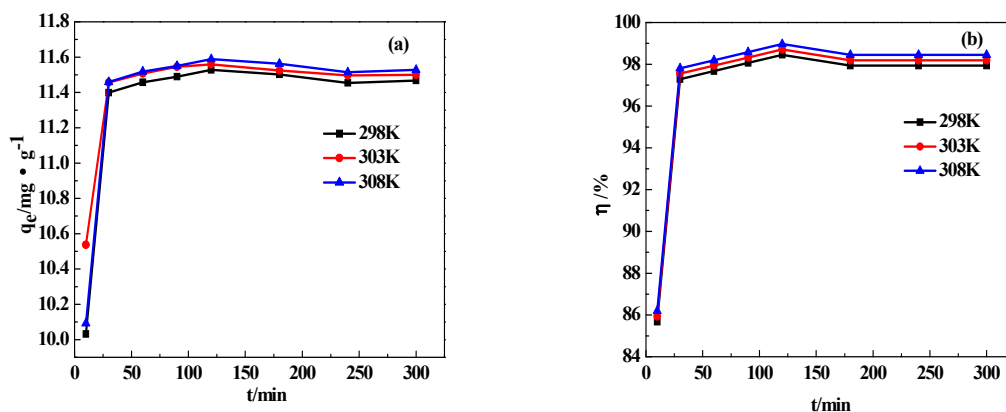


Figure 17. Effect of adsorption time on adsorption amount (a) and adsorption removal rate (b).

The adsorption isotherm reflects the distribution of the solid-phase and liquid-phase when the solute molecules adsorbed at a certain temperature when reaching equilibrium on the two phases interface. The adsorption isotherm of CDG for AY11 at different temperatures is shown in Figure 14. The figure shows that when the initial concentration of AY11 increases within a certain range, the equilibrium concentration of AY11 molecules in CDG and solution shows an increasing trend after attaining the adsorption equilibrium. When the amount of Ay11 molecules in the solid phase CDG reaches a certain value, the adsorbate was no longer distributed into the adsorbent, but distributed into the liquid phase, indicating that the adsorbent reached adsorption saturation. The distribution of adsorbate into the adsorbent increases while elevating the temperature, and the equilibrium adsorption of Ay11 by CDG increased continuously because the diffusion rate of AY11 molecules into the CDG increased continuously with the increase in temperature, indicating that the adsorption of AY11 was an endothermic process.

It can be seen from Figure 18 that the adsorption of AY11 dye onto CDG conforms to the quasi-first-order kinetic model, and from Table 3, the correlation coefficient of the quasi-first-order kinetic model, namely $R^2 > 0.99$, and the adsorption rate constant k_1 with temperature can be observed, which shows that there is a chemical bond between the adsorbent and the adsorbate [65].

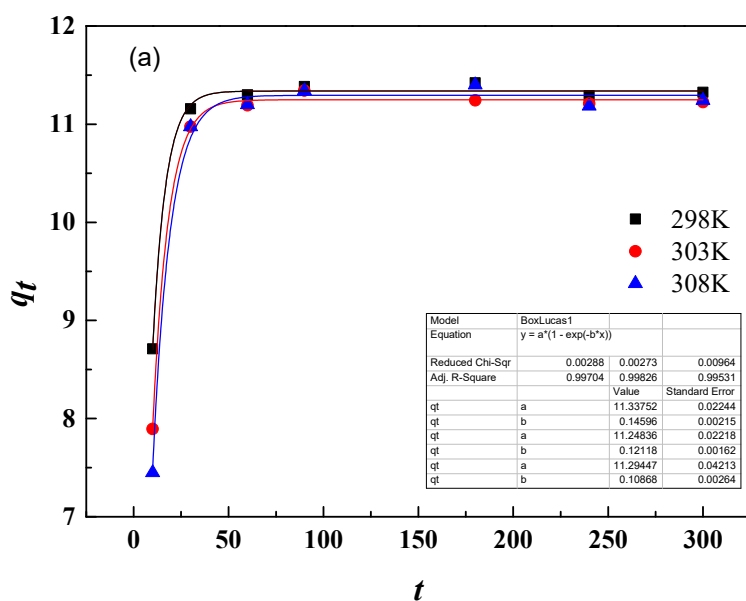


Figure 18. Cont.

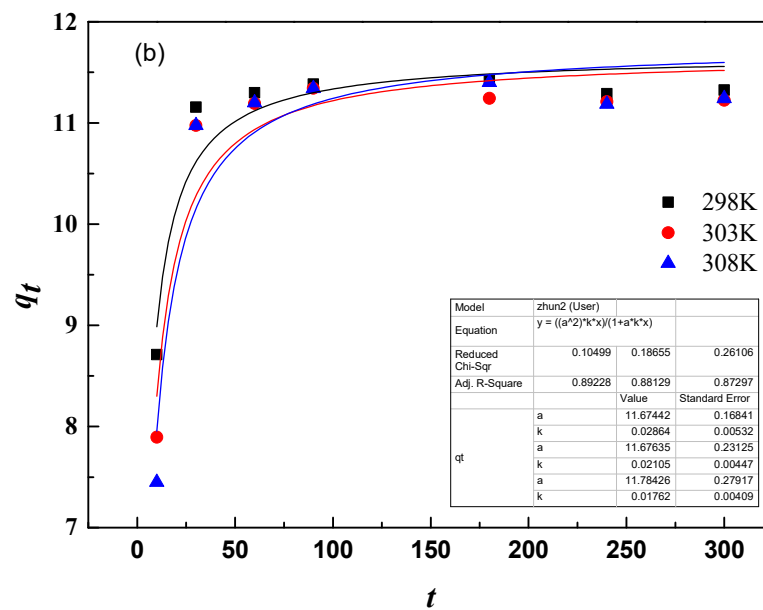


Figure 18. (a) Quasi-first-order nonlinear and (b) quasi-second-order nonlinear dynamics model.

Table 3. Dynamic characteristic parameters of pseudo-first-order and pseudo-second-order models at different temperatures.

T/K	$q_{e,exp}/(\text{mg/g})$	First-Order Kinetic Model			Second-Order Kinetic Model		
		k_1/min^{-1}	$q_{e,cal}/(\text{mg/g})$	R^2	$k_2/[\text{g} \cdot (\text{mg} \cdot \text{min})^{-1}]$	$q_{e,cal}/(\text{mg/g})$	R^2
298 K	11.33	0.146	11.34	0.997	0.029	11.67	0.892
303 K	11.56	0.121	11.25	0.998	0.021	11.68	0.881
308 K	11.59	0.109	11.29	0.995	0.018	11.78	0.873

3.9.2. Adsorption Isotherm

Based on the fitting curve and regression parameters of the Langmuir equation and the linear Freundlich diffusion model (Figure 19a,b and Table 4), the regression coefficient (R^2) of the nonlinear Langmuir and Freundlich equation was higher than 0.93 at the temperature range from 298 K to 308 K. Compared to the Freundlich adsorption equation, Langmuir R^2 was always above 0.97, indicating that the adsorption equilibria relationship between CDG and AY11 molecules can be more accurately described by the Langmuir equation. The Langmuir adsorption model assumed that the molecular adsorption was a monolayer surface adsorption, and the adsorption surface was uniform, containing a few identical sites. The adsorbed particles were completely independent without interaction.

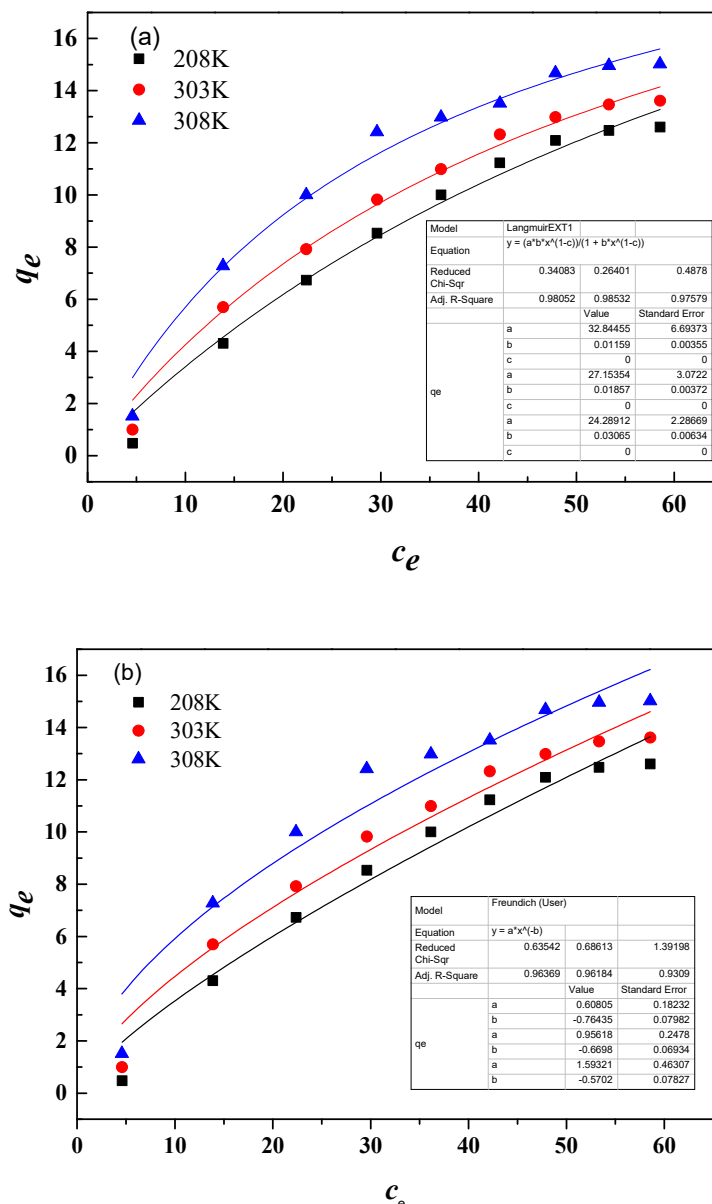


Figure 19. (a) Langmuir and (b) Freundlich adsorption isotherm models.

Table 4. Adsorption isotherm model parameters of Langmuir and Freundlich model at different temperatures.

T(K)	Langmuir Equation			Freundlich Equation		
	$q_m/(mg/g)$	$K_L/(mL/g)$	R^2	$K_F/(mg/g)$	$1/n$	R^2
298	32.84	0.0116	0.9805	0.6081	0.76	0.9637
303	27.15	0.0186	0.9853	0.9562	0.67	0.9618
308	24.30	0.0307	0.9758	1.5932	0.57	0.9309

3.9.3. Adsorption Thermodynamics

It can be observed from Figure 20 and Table 5 that $\Delta G_0 < 0$, and the value is between -20 kJ/mol and 0, which indicates that the adsorption behavior of CDG on AY11 is spontaneous and is physical adsorption [66]. The change in the standard entropy ($\Delta S_0 < 0$), indicated that the degree of order at the solid–liquid interface increases during the adsorption process. The values of $\Delta H_0 > 0$ indicate that the adsorption process is endothermic,

and increasing the temperature is conducive to the adsorption behavior. This can also be verified from the adsorption data of CDG on AY11 at different temperatures (Figure 9). Therefore, it can be concluded that the process of CDG adsorption of AY11 has not only chemical adsorption but also physical adsorption.

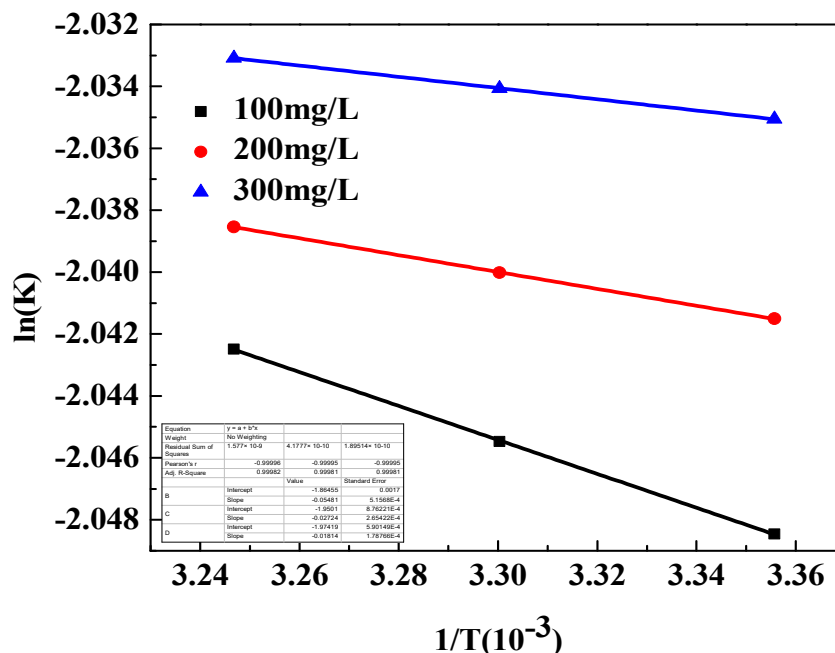


Figure 20. Thermodynamic model of CDG adsorption on AY11 at different initial concentrations of AY11.

Table 5. Thermodynamic parameters at different initial concentrations of AY11.

C ₀ /(mg/L)	ΔH ₀ /(kJ·mol ⁻¹)	ΔS ₀ /(J·mol ⁻¹ ·K)	ΔG ₀ /(kJ·mol ⁻¹)		
			298 K	303 K	308 K
100	0.46	-15.50	-5.08	-5.06	-5.04
200	0.23	-16.21	-5.15	-5.14	-5.12
300	0.15	-16.41	-5.23	-5.22	-5.21

3.9.4. Adsorption Model

Dye adsorption and removal are usually characterized as four consecutive steps [67,68]: (1) dye molecules from an aqueous solution are close to the outer surface of the adsorbent; (2) mass transfer across the boundary layer (membrane diffusion); (3) dye molecules diffusion within the particles in the pores of the adsorbent (pore diffusion); and (4) adsorption of dye molecules on the surface of the adsorbent through molecular interaction (reaction).

Figure 21 presents a schematic representation of the adsorption process of CDG and AY11, in which the first stage is rapid adsorption; the second stage is slow adsorption until reaching saturation; and the third stage is adsorption equilibrium. Among them, the concentration of the dye and the stirring speed may affect the first step, so in the thoroughly mixed batch adsorption, step 1 is very fast, and is therefore called the rapid adsorption stage. In most of the cases, steps 2 and 3 could mainly control the adsorption rate, while external and internal diffusion is usually regarded as an essential step to determine the adsorption rate.

Figure 22 shows the adsorption mechanism of AY11 dye by CDG. It can be seen that the dye diffuses into the adsorbent through pores. During the next step, AY11 ionizes out -SO₃⁻ in water and electrostatically interacts with the -N + (CH₃)₃ group on the surface of CDG. Therefore, AY11 molecules can reach the surface of CDG and could enter the pores

of CDG, as an establishment of a stronger chemical bond with AY11 is more conducive to the adsorption process. This process is mainly affected by the mass transfer resistance of the CDG surface, which slows down the adsorption process. The second stage, is the gradual adsorption stage, but this is not the only rate control step, as external mass transfer or ion exchange may also be involved in the adsorption process [69,70]. With the increase in time, more and more $-SO_3^-$ of AY11 molecules could participate in the competition, resulting in the reduction of the adsorption sites on the surface of CDG, which slows down the adsorption rate and eventually reaches adsorption equilibrium.

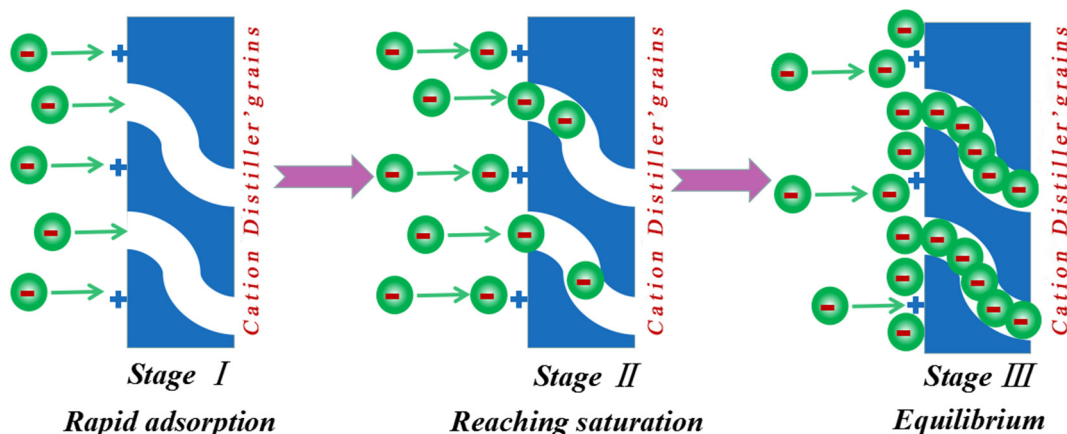


Figure 21. Schematic representation of the adsorption process of CDG and AY11.

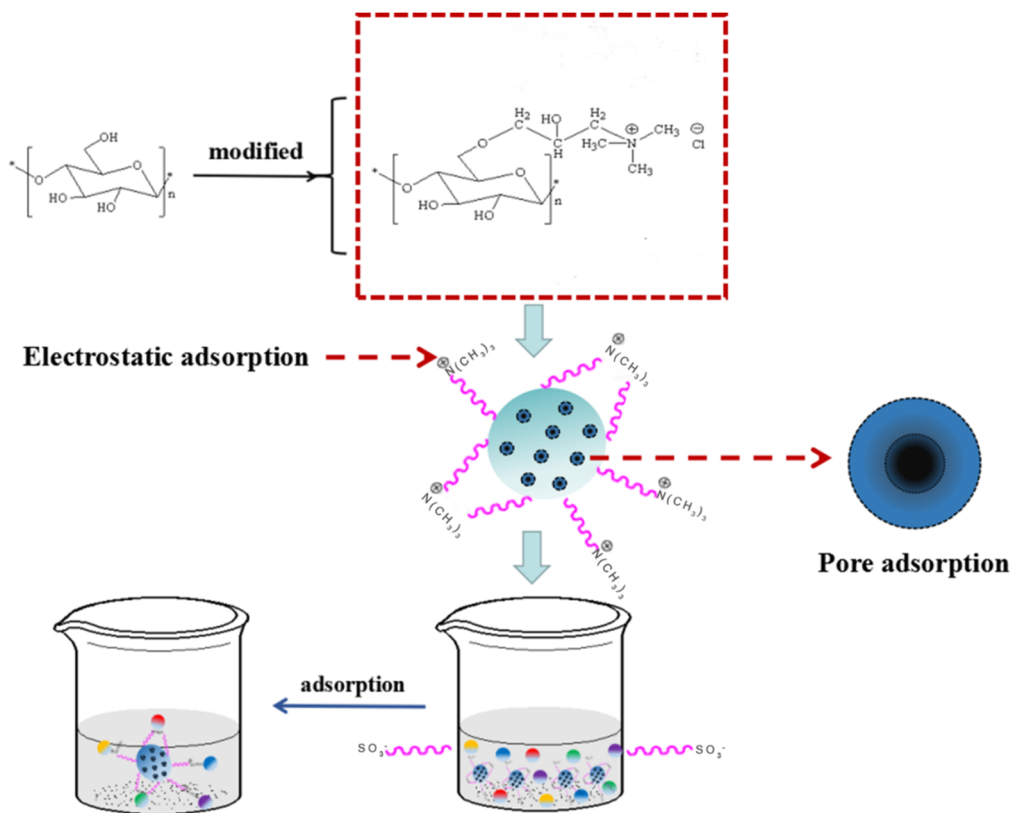


Figure 22. The adsorption mechanism of AY11 on CDG (* the terminal group).

3.10. Comparison of Various Adsorbents

Table 6 shows the comparison of the maximum adsorption capacity of anionic azo dyes on various adsorbents. It can be seen from Table 6 that the maximum adsorption

capacity of anionic azo dyes on CDG is 636.94 mg g^{-1} , which is much higher than other clay and polymer materials under optimal adsorption conditions. Therefore, CDG is a promising material for treating anionic azo dyes from dye wastewater.

Table 6. Comparison of maximum adsorption capacity of adsorbents.

Adsorbent	Dye	Optimum Adsorption Conditions	MG Adsorption q_{\max} (mg/g)	Reference
Fe-coated pumice stone	Acid orange 7	3.2 g/L; 120 min; pH = 7; 24 °C	27.68	[71]
Surfactant-coated zeolite	Acid orange 7	4.0 g/L; 60 min; pH = 1; 30 °C	38.96	[72]
Potash alum doped polyaniline	Acid orange 7	1.6 g/L; 100 min; pH = 7; 25 °C	99	[73]
	Metanil yellow	1.6 g/L; 100 min; pH = 7; 25 °C	142	
Amino functionalized graphenes	Metanil yellow	0.4 g/L; 120 min; pH = 7; 25 °C	71.62	[74]
Polyaniline-bentonite composite	Metanil yellow	1.0 g/L; 240 min; pH = 7; 25 °C	444.4	[75]
Polyacrylonitrile/activated carbon composite	Acid yellow 99	0.4 g/L; 60 min; pH = 1; 50 °C	217.39	[76]
Magnetic gelatin-biocomposite	Direct Yellow 12	0.1 g/L; 240 min; pH = 3; 30 °C	476.2	[77]
[Cu ₂ -L]@MWCNT	Sunset yellow	0.01 g/L; 120 min; pH = 7; 30 °C	26.63	[78]
Cationic distiller's grains (CDG)	Acid yellow 11	8.5 g/L; 180 min; pH = 7; 25 °C	636.94	This study

4. Conclusions

Using the alkali pre-treatment and CHPTAC etherification modification method, the waste of distillers grains were successfully transformed into quaternary ammonium cation distillers grain adsorbent (CDG). FTIR spectrum analysis and EDS elements analysis showed that CHPTAC successfully modified the DGs. BET analysis of CDG showed that a large number of pore structures appeared on the surface of CDG, which provided a large number of adsorption sites for the attachment of Acid yellow 11 (AY11). UV-Vis spectrometry showed that CDG had an excellent removal rate of AY11. Batch adsorption experiments showed that the optimal adsorption conditions for CDG to adsorb AY11 dye in aqueous solution are an adsorption temperature of 25 °C, an adsorption time of 180 min, amount of adsorbent at 8.5 g/L, initial concentration of AY11 100 mg/L, and the pH of the AY11 solution has to be set at 7.0. Under optimal conditions, the maximum adsorption removal rate of CDG for AY11 is 98.76%, and after eight adsorption-desorption experiments, the adsorption removal rate was still higher than 81%. Moreover, it is more likely to be used in the actual treatment of azo dye wastewater to realize the sustainable environmental protection concept of energy-saving and emission reduction. Zeta potential, adsorption kinetics, and adsorption thermodynamics results showed that the adsorption process of CDG to AY11 was mainly chemical adsorption. To summarise, CDG could be used as a potential adsorbent for azo dye wastewater treatment.

Author Contributions: Conceptualization, C.L. and C.W.; methodology, D.K. and X.M.; resources, H.W.; writing—original draft preparation, D.K. and X.M.; writing—review and editing, D.K.; funding acquisition, X.Y., C.W. and H.W. All authors have read and agreed to the published version of the manuscript.

Funding: This research was funded by the Open Research Fund Program of Key Laboratory of Cleaner Production and Integrated Resource Utilization of China National Light Industry (CP-2018-YB2), Liquor making Biological Technology and Application of key laboratory of Sichuan Province (NJ2019-01), Key Laboratory of Wuliangye-flavor Liquor Solid-state Fermentation, China National Light Industry (2018JJ005).

Institutional Review Board Statement: Not applicable.

Informed Consent Statement: Not applicable.

Data Availability Statement: Not applicable.

Acknowledgments: Financial support for this work was provided by the Open Research Fund Program of Key Laboratory of Cleaner Production and Integrated Resource Utilization of China National Light Industry (CP-2018-YB2), Liquor making Biological Technology and Application of key laboratory of Sichuan Province (NJ2019-01), Key Laboratory of Wuliangye-flavor Liquor Solid-state Fermentation, China National Light Industry (2018zd010), Key Science and Technology Project of Zigong City (2019YYJC28).

Conflicts of Interest: The authors declare no conflict of interest.

References

1. Iqbal, M.; Abbas, M.; Nisar, J.; Nazir, A. Bioassays based on higher plants as excellent dosimeters for ecotoxicity monitoring: A review. *Chem. Int.* **2019**, *5*, 1–80.
2. Abbas, M.; Adil, M.; Ehtisham-Ul-Haque, S.; Munir, B.; Yameen, M.; Ghaffar, A.; Shar, G.A.; Tahir, M.A.; Iqbal, M. Vibrio fischeri bioluminescence inhibition assay for ecotoxicity assessment: A review. *Sci. Total Environ.* **2018**, *626*, 1295–1309. [[CrossRef](#)]
3. Iqbal, M. Vicia faba bioassay for environmental toxicity monitoring: A review. *Chemosphere* **2016**, *144*, 785–802. [[CrossRef](#)]
4. Siddiqua, U.H.; Ali, S.; Iqbal, M.; Hussain, T. Relationship between structure and dyeing properties of reactive dyes for cotton dyeing. *J. Mol. Liq.* **2017**, *241*, 839–844. [[CrossRef](#)]
5. Shah, N.S.; Khan, J.A.; Sayed, M.; Khan, Z.U.H.; Iqbal, J.; Arshad, S.; Junaid, M.; Khan, H.M. Synergistic effects of H₂O₂ and S₂O₈²⁻ in the gamma radiation induced degradation of congo-red dye: Kinetics and toxicities evaluation. *Sep. Purif. Technol.* **2020**, *233*, 115966. [[CrossRef](#)]
6. Dai, H.; Huang, Y.; Huang, H. Eco-friendly polyvinyl alcohol/carboxymethyl cellulose hydrogels reinforced with graphene oxide and bentonite for enhanced adsorption of methylene blue. *Carbohydr. Polym.* **2018**, *185*, 1–11.
7. Liu, H.; Guo, W.; Li, Y.; He, S.; He, C. Photocatalytic degradation of sixteen organic dyes by TiO₂/WO₃-coated magnetic nanoparticles under simulated visible light and solar light. *J. Chem. Environ. Eng.* **2018**, *6*, 59–67. [[CrossRef](#)]
8. Sinha, A.; Lulu, S.; Vino, S.; Banerjee, S.; Acharjee, S.; Osborne, W.J. Degradation of reactive green dye and textile effluent by Candida sp. VITJASS isolated from wetland paddy rhizosphere soil. *J. Environ. Chem. Eng.* **2018**, *6*, 5150–5159. [[CrossRef](#)]
9. Liu, S.; Wang, Z.; Li, J.; Zhao, C.; He, X.; Yang, G. Fabrication of slag particle three-dimensional electrode system for methylene blue degradation: Characterization, performance and mechanism study. *Chemosphere* **2018**, *213*, 377–383. [[CrossRef](#)]
10. Obiora-Okafo, I.A.; Onukwuli, O.D. Characterization and optimization of spectrophotometric colour removal from dye containing wastewater by Coagulation-Flocculation. *Pol. J. Chem. Technol.* **2018**, *20*, 49–59. [[CrossRef](#)]
11. Wolski, L.; Walkowiak, A.; Ziolk, M. Formation of reactive oxygen species upon interaction of Au/ZnO with H₂O₂ and their activity in methylene blue degradation. *Catal. Today* **2019**, *333*, 54–62. [[CrossRef](#)]
12. Criscuoli, A.; Zhong, J.; Figoli, A.; Carnevale, M.; Huang, R.; Drioli, E. Treatment of dye solutions by vacuum membrane distillation. *Water Res.* **2008**, *42*, 5031–5037. [[CrossRef](#)]
13. Zhang, B.; Dong, Z.; Sun, D.; Wu, T.; Li, Y. Enhanced adsorption capacity of dyes by surfactant-modified layered double hydroxides from aqueous solution. *J. Ind. Eng. Chem.* **2017**, *49*, 208–218. [[CrossRef](#)]
14. Tian, S.; Xu, S.; Liu, J.; He, C.; Xiong, Y.; Feng, P. Highly efficient removal of both cationic and anionic dyes from wastewater with a water-stable and eco-friendly Fe-MOF via host-guest encapsulation. *J. Clean. Prod.* **2019**, *239*, 117767. [[CrossRef](#)]
15. Shanmugam, M.; Alsalmeh, A.; Alghamdi, A.; Jayavel, R. Enhanced Photocatalytic Performance of the Graphene-V₂O₅ Nanocomposite in the Degradation of Methylene Blue Dye under Direct Sunlight. *ACS Appl. Mater. Interfaces* **2015**, *7*, 14905–14911. [[CrossRef](#)]
16. Kabdaşlı, I.; Bilgin, A.; Tünay, O.; Kabdaşlı, I. Sulphate control by ettringite precipitation in textile industry wastewaters. *Environ. Technol.* **2015**, *37*, 446–451. [[CrossRef](#)]
17. Wawrzekiewicz, M.; Wiśniewska, M.; Wołowicz, A.; Gun'ko, V.M.; Zarko, V.I. Mixed silica-alumina oxide as sorbent for dyes and metal ions removal from aqueous solutions and wastewaters. *Microporous Mesoporous Mater.* **2017**, *250*, 128–147. [[CrossRef](#)]
18. Xu, Y.; Li, Z.; Su, K.; Fan, T.; Cao, L. Mussel-inspired modification of PPS membrane to separate and remove the dyes from the wastewater. *Chem. Eng. J.* **2018**, *341*, 371–382. [[CrossRef](#)]
19. Mohammed, N.; Grishkewich, N.; Waeijen, H.A.; Berry, R.M.; Tam, K.C. Continuous flow adsorption of methylene blue by cellulose nanocrystal-alginate hydrogel beads in fixed bed columns. *Carbohydr. Polym.* **2016**, *136*, 1194–1202. [[CrossRef](#)]

20. Wawrzkiwicz, M.; Wiśniewska, M.; Gun'ko, V.M.; Zarko, V.I. Adsorptive removal of acid, reactive and direct dyes from aqueous solutions and wastewater using mixed silicacalumina oxide. *Powder Technol.* **2015**, *278*, 306–315. [[CrossRef](#)]
21. Gładysz-Płaska, A.; Skwarek, E.; Budnyak, T.M.; Kołodzyńska, D. Metal Ions Removal Using Nano Oxide Pyrolox™ Material. *Nanoscale Res. Lett.* **2017**, *12*, 95. [[CrossRef](#)]
22. Du, H.; Cheng, J.; Wang, M.; Tian, M.; Yang, X.; Wang, Q. Red dye extracted sappan wood waste derived activated carbons characterization and dye adsorption properties. *Diam. Relat. Mater.* **2020**, *102*, 107646. [[CrossRef](#)]
23. Panda, J.; Sahoo, J.K.; Panda, P.K.; Sahu, S.N.; Samal, M.; Pattanayak, S.K.; Sahu, R. Adsorptive behavior of zeolitic imidazolate framework-8 towards anionic dye in aqueous media: Combined experimental and molecular docking study. *J. Mol. Liq.* **2019**, *278*, 536–545. [[CrossRef](#)]
24. Pisareva, A.S.; Tikhomirova, T.I. Sorption of Synthetic Anionic Amaranth Dye from an Aqueous Solution on Hydrophobized Silica and Alumina. *Russ. J. Phys. Chem. A* **2019**, *93*, 534–537. [[CrossRef](#)]
25. Baliś, A.; Id, S.Z. Tailored synthesis of core-shell mesoporous silica particles—Optimization of dye sorption properties. *Nanomaterials* **2018**, *8*, 230. [[CrossRef](#)]
26. Luensmann, D.; Jones, L. Impact of fluorescent probes on albumin sorption profiles to ophthalmic biomaterials. *J. Biomed. Mater. Res. Part B Appl. Biomater.* **2010**, *94*, 327–336. [[CrossRef](#)]
27. Wu, B.; Zhang, W.-H.; Ren, Z.-G.; Lang, J.-P. A 1D anionic coordination polymer showing superior Congo Red sorption and its dye composite exhibiting remarkably enhanced photocurrent response. *Chem. Commun.* **2015**, *51*, 14893–14896. [[CrossRef](#)]
28. Malik, P.K. Use of activated carbons prepared from sawdust and rice-husk for adsorption of acid dyes: A case study of Acid Yellow 36. *Dye. Pigment.* **2003**, *56*, 239–249. [[CrossRef](#)]
29. Ahmad, A.A.; Hameed, B.H. Fixed-bed adsorption of reactive azo dye onto granular activated carbon prepared from waste. *J. Hazard. Mater.* **2010**, *175*, 298–303. [[CrossRef](#)]
30. Gupta, V.K.; Gupta, B.; Rastogi, A.; Agarwal, S.; Nayak, A. A comparative investigation on adsorption performances of mesoporous activated carbon prepared from waste rubber tire and activated carbon for a hazardous azo dye—Acid Blue 113. *J. Hazard. Mater.* **2011**, *186*, 891–901. [[CrossRef](#)]
31. Ríos-Gómez, J.; Ferrer-Monteagudo, B.; López-Lorente, Á.I.; Lucena, R.; Luque, R.; Cárdenas, S. Efficient combined sorption/photobleaching of dyes promoted by cellulose/titania-based nanocomposite films. *J. Clean. Prod.* **2018**, *194*, 167–173. [[CrossRef](#)]
32. Sun, X.; Yang, L.; Li, Q.; Zhao, J.; Li, X.; Wang, X.; Liu, H. Amino-functionalized magnetic cellulose nanocomposite as adsorbent for removal of Cr(VI): Synthesis and adsorption studies. *Chem. Eng. J.* **2014**, *241*, 175–183. [[CrossRef](#)]
33. Sarsenov, A.; Bishimbaev, V.; Kapsalamov, B.; Lepesov, K.; Gapparova, K.; Grzesiak, P. Chemical modification of cellulose for boron sorption from water solutions. *Pol. J. Chem. Technol.* **2018**, *20*, 123–128. [[CrossRef](#)]
34. Villegas-Torres, M.F.; Ward, J.M.; Lye, G.J. The protein fraction from wheat-based dried distiller's grain with solubles (DDGS): Extraction and valorization. *New Biotechnol.* **2015**, *32*, 606–611. [[CrossRef](#)]
35. Zhang, X.Y.; Tan, J.; Wei, X.H.; Wang, L.J. Removal of Remazol turquoise Blue G-133 from aqueous solution using modified waste newspaper fiber. *Carbohydr. Polym.* **2013**, *92*, 1497–1502. [[CrossRef](#)]
36. Hashem, A.M.A.; El-Shishtawy, R.M. Preparation and Characterization of Cationized Cellulose for the Removal of Anionic Dyes. *Adsorpt. Sci. Technol.* **2001**, *19*, 197–210. [[CrossRef](#)]
37. Qi, Y.; Li, J.; Wang, L.J. Removal of Remazol Turquoise Blue G-133 from aqueous medium using functionalized cellulose from recycled newspaper fiber. *Ind. Crop. Prod.* **2013**, *50*, 15–22. [[CrossRef](#)]
38. Idan, I.J.; Abdullah, L.C.; Mahdi, D.S.; Obaid, M.K.; Jamil, S.N.A.B.M. Adsorption of Anionic Dye Using Cationic Surfactant-Modified Kenaf Core Fibers. *Open Access Libr. J.* **2017**, *4*, 1. [[CrossRef](#)]
39. Khy, A.; Pj, A.; Kbr, B.; Sumant, A.V.; Skoog, S.A.; Narayan, R.J. Correlation of zeta potential and contact angle of oxygen and fluorine terminated nitrogen incorporated ultrananocrystalline diamond (N-UNCD) thin films. *Mater. Lett.* **2021**, *295*, 129823.
40. Cheng, F.; Zhou, X.; Zhang, J.; Lu, L.; Ma, J. Effects of cations on the adsorption kinetics of bt protein on mineral surfaces. *J. Agro-Environ. Sci.* **2017**, *9*, 1844–1849.
41. Lei, S.; Li, X. Adsorption and degradation of 1,2,4-trichlorobenzene by activated carbon-microorganisms in soil. *J. Agro-Environ. Sci.* **2015**, *8*, 1535–1541.
42. Zou, W.; Zhao, L.; Han, R. Adsorption characteristics of uranyl ions by manganese oxide coated sand in batch mode. *J. Radioanal. Nucl. Chem.* **2011**, *288*, 239–249. [[CrossRef](#)]
43. Aksu, Z.; Tezer, S. Biosorption of reactive dyes on the green alga *Chlorella vulgaris*. *Process Biochem.* **2005**, *40*, 1347–1361. [[CrossRef](#)]
44. Bergaoui, M.; Nakhli, A.; Benguerba, Y.; Khalfoui, M.; Erto, A.; Soetaredjo, F.E.; Ismadji, S.; Ernst, B. Novel insights into the adsorption mechanism of methylene blue onto organo-bentonite: Adsorption isotherms modeling and molecular simulation. *J. Mol. Liq.* **2018**, *272*, 697–707. [[CrossRef](#)]
45. Ayawei, N.; Ebelegi, A.N.; Wankasi, D. Modelling and interpretation of adsorption isotherms. *J. Chem.* **2017**, *2017*, 3039817. [[CrossRef](#)]
46. Elwakeel, K.Z.; Guibal, E. Arsenic(V) sorption using chitosan/Cu(OH)₂ and chitosan/CuO composite sorbents. *Carbohydr. Polym.* **2015**, *134*, 190–204. [[CrossRef](#)]

47. Bao, S.Y.; Tang, L.H.; Li, K.; Ning, P.; Peng, J.H.; Guo, H.B.; Zhu, T.T.; Liu, Y. Highly selective removal of Zn(II) ion from hot-dip galvanizing pickling waste with amino-functionalized Fe₃O₄@SiO₂, magnetic nano-adsorbent. *J. Colloid Interface Sci.* **2016**, *462*, 235–242. [[CrossRef](#)]
48. Ren, Y.; Abbood, H.A.; He, F.; Peng, H.; Huang, K. Magnetic EDTA-modified chitosan/SiO₂/Fe₃O₄, adsorbent: Preparation, characterization, and application in heavy metal adsorption. *Chem. Eng. J.* **2013**, *226*, 300–311. [[CrossRef](#)]
49. Bajaj, K.; Sakhuja, R. *Benzotriazole: Much More than Just Synthetic Heterocyclic Chemistry*; The Chemistry of Benzotriazole Derivatives; Springer International Publishing: Berlin/Heidelberg, Germany, 2015.
50. Lonappan, L.; Rouissi, T.; Brar, S.K.; Verma, M.; Surampalli, R.Y. An insight into the adsorption of diclofenac on different biochars: Mechanisms, surface chemistry, and thermodynamics. *Bioresour. Technol.* **2018**, *249*, 386–394. [[CrossRef](#)]
51. Hokkanen, S.; Bhatnagar, A.; Sillanpaa, M. A review on modification methods to cellulose-based adsorbents to improve adsorption capacity. *Water Res.* **2016**, *91*, 156–173. [[CrossRef](#)]
52. Park, K.-H.; Yu, S.-H.; Kim, H.-S.; Park, H.-D. Inhibition of biofouling by modification of forward osmosis membrane using quaternary ammonium cation. *Water Sci. Technol.* **2015**, *72*, 738–745. [[CrossRef](#)] [[PubMed](#)]
53. Wang, C.; Jin, J.; Sun, Y.; Yao, J.; Zhao, G.; Liu, Y. In-situ synthesis and ultrasound enhanced adsorption properties of MoS₂/graphene quantum dot nanocomposite. *Chem. Eng. J.* **2017**, *327*, 774–782. [[CrossRef](#)]
54. Zhang, T.; Zhang, K.; Li, J.; Yue, X. Simultaneously enhancing hydrophilicity, chlorine resistance and anti-biofouling of APA-TFC membrane surface by densely grafting quaternary ammonium cations and salicylaldehydes. *J. Membr. Sci.* **2017**, *528*, 296–302. [[CrossRef](#)]
55. Choi, A.E.S.; Roces, S.; Dugos, N.; Arcega, A.; Wan, M.W. Adsorptive removal of dibenzothiophene sulfone from fuel oil using clay material adsorbents. *J. Clean. Prod.* **2017**, *161*, 267–276. [[CrossRef](#)]
56. Değermenci, G.D.; Değermenci, N.; Ayvaoğlu, V.; Durmaz, E.; Çakır, D.; Akan, E. Adsorption of reactive dyes on lignocellulosic waste; characterization, equilibrium, kinetic and thermodynamic studies. *J. Clean. Prod.* **2019**, *225*, 1220–1229. [[CrossRef](#)]
57. Li, C.; Wu, N.; Zhang, M.; Wei, C.; Yan, F.; Wang, Z. Effects of E44 and KH560 modifiers on properties of distillers grains poly(butylene succinate) composites. *Polym. Compos.* **2018**, *40*, 1499–1509. [[CrossRef](#)]
58. Wang, B.; Lian, G.; Lee, X.; Gao, B.; Li, L.; Liu, T.; Zhang, X.; Zheng, Y. Phosphogypsum as a novel modifier for distillers grains biochar removal of phosphate from water. *Chemosphere* **2020**, *238*, 124684. [[CrossRef](#)]
59. Oliveira, K.R.; Segura, J.G.; Oliveira, B.A.; Medeiros, A.C.L.; Zimba, R.D.; Viegas, E.M. Distillers' dried grains with soluble in diets for Pacu, *Piaractus mesopotamicus* juveniles: Growth performance, feed utilization, economic viability, and phosphorus release. *Anim. Feed. Sci. Technol.* **2020**, *262*, 114393. [[CrossRef](#)]
60. Lee, C.; Morris, D.L.; Lefever, K.M.; Dieter, P.A. Feeding a diet with corn distillers grain with solubles to dairy cows alters manure characteristics and ammonia and hydrogen sulfide emissions from manure. *J. Dairy Sci.* **2020**, *103*, 2363–2372. [[CrossRef](#)]
61. Zhang, Z.; Wang, Q.; Li, L.; Xu, G. Pyrolysis characteristics, kinetics and evolved volatiles determination of rice-husk-based distiller's grains. *Biomass Bioenergy* **2020**, *135*, 105525. [[CrossRef](#)]
62. Thommes, M.; Guillet-Nicolas, R.; Cychosz, K.A. *Physical Adsorption Characterization of Mesoporous Zeolites. Mesoporous Zeolites*; John Wiley & Sons, Ltd.: Hoboken, NJ, USA, 2015; pp. 349–384.
63. Sadeek, S.A.; Negm, N.; Hefni, H.; Wahab, M.M.A. Metal adsorption by agricultural biosorbents: Adsorption isotherm, kinetic and biosorbents chemical structures. *Int. J. Biol. Macromol.* **2015**, *81*, 400–409. [[CrossRef](#)] [[PubMed](#)]
64. Chakraborty, R.; Verma, R.; Asthana, A.; Vidya, S.S.; Singh, A.K. Adsorption of hazardous chromium (VI) ions from aqueous solutions using modified sawdust: Kinetics, isotherm and thermodynamic modelling. *Int. J. Environ. Anal. Chem.* **2019**, *101*, 911–928. [[CrossRef](#)]
65. Wang, Y.; Zhang, C.; Zhao, L.; Meng, G.; Wu, J.; Liu, Z. Cellulose-based porous adsorbents with high capacity for methylene blue adsorption from aqueous solutions. *Fibers Polym.* **2017**, *8*, 891–899. [[CrossRef](#)]
66. Battirolo, L.C.; Zanata, D.M.; Gon Alves, M.C. Improvement of cellulose acetate dimensional stability by chemical crosslinking with cellulose nanocrystals. *Compos. Part A Appl. Sci. Manuf.* **2018**, *113*, 105–113. [[CrossRef](#)]
67. Crittenden, J.C.; Trussell, R.R.; Hand, D.W.; Howe, K.J.; Tchobanoglous, G. *MWH's Water Treatment: Principles and Design*, 3rd ed.; John Wiley & Sons Inc.: Hoboken, NJ, USA, 2012.
68. Firdaous, L.; Fertin, B.; Khelissa, O.; Dhainaut, M.; Nedjar, N.; Chataigné, G.; Ouhoud, L.; Lutin, F.; Dhulster, P. Adsorptive removal of polyphenols from an alfalfa white proteins concentrate: Adsorbent screening, adsorption kinetics and equilibrium study. *Sep. Purif. Technol.* **2017**, *178*, 29–39. [[CrossRef](#)]
69. Albadarin, A.B.; Mangwandi, C.; Al-Muhtaseb, A.H.; Walker, G.M.; Allen, S.J.; Ahmad, M.N. Kinetic and thermodynamics of chromium ions adsorption onto low-cost dolomite adsorbent. *Chem. Eng. J.* **2012**, *179*, 193–202. [[CrossRef](#)]
70. Wu, Z.; Zhong, H.; Yuan, X.; Wang, H.; Wang, L.; Chen, X.; Zeng, G.; Wu, Y. Adsorptive removal of methylene blue by rhamnolipid-functionalized graphene oxide from wastewater. *Water Res.* **2014**, *67*, 330–344. [[CrossRef](#)]
71. Heibati, B.; Rodriguez-Couto, S.; Turan, N.G.; Ozgonenel, O.; Albadarin, A.B.; Asif, M.; Tyagi, I.; Agarwal, S.; Gupta, V.K. Removal of noxious dye—Acid Orange 7 from aqueous solution using natural pumice and Fe-coated pumice stone. *J. Ind. Eng. Chem.* **2015**, *31*, 124–131. [[CrossRef](#)]
72. Jin, X.; Yu, B.; Chen, Z.; Arocena, J.M.; Thring, R.W. Adsorption of Orange II dye in aqueous solution onto surfactant-coated zeolite: Characterization, kinetic and thermodynamic studies. *J. Colloid Interface Sci.* **2014**, *435*, 15–20. [[CrossRef](#)]

73. Patra, B.N.; Majhi, D. Removal of Anionic Dyes from Water by Potash Alum Doped Polyaniline: Investigation of Kinetics and Thermodynamic Parameters of Adsorption. *J. Phys. Chem. B* **2015**, *119*, 8154–8164. [[CrossRef](#)]
74. Guo, X.; Wei, Q.; Du, B.; Zhang, Y.; Xin, X.; Yan, L.; Yu, H. Removal of Metanil Yellow from water environment by amino functionalized graphenes (NH₂-G)—Influence of surface chemistry of NH₂-G. *Appl. Surf. Sci.* **2013**, *284*, 862–869. [[CrossRef](#)]
75. Meng, F.; Wang, L.; Pei, M.; Guo, W.; Liu, G. Adsorption of metanil yellow from aqueous solution using polyaniline-bentonite composite. *Colloid Polym. Sci.* **2017**, *295*, 1165–1175. [[CrossRef](#)]
76. El-Bindary, A.A.; Hussien, M.A.; Diab, M.A.; Eessa, A.M. Adsorption of Acid Yellow 99 by polyacrylonitrile/activated carbon composite: Kinetics, thermodynamics and isotherm studies. *J. Mol. Liq.* **2014**, *197*, 236–242. [[CrossRef](#)]
77. Amooey, A.A.; Alinejad-Mir, A.; Ghasemi, S.; Marzbali, M.H. The removal of Direct Yellow 12 from synthetic aqueous solution by a novel magnetic nanobioadsorbent. *Int. J. Environ. Sci. Technol.* **2019**, *16*, 8343–8354. [[CrossRef](#)]
78. El-Sharkawy, R.; El-Ghamry, H.A. Multi-walled carbon nanotubes decorated with Cu(II) triazole Schiff base complex for adsorptive removal of synthetic dyes. *J. Mol. Liq.* **2019**, *282*, 515–526. [[CrossRef](#)]